Solid Freeform Fabrication 2024: Proceedings of the 35th Annual International Solid Freeform Fabrication Symposium – An Additive Manufacturing Conference
Reviewed Paper

PLA-HA/BBG Composite Scaffolds Fabricated by Digital-Light-Processing 3D Printing for Cranial Bone Regeneration

E. Gepek[1, 2, 3], F. Fayyazbakhsh[2, 4], O. Iyibilgin[3, 5], L. Suliandziga[2] and M. C. Leu[2, 4]

[1] Sakarya University, Institute of Natural Sciences, 54187 Sakarya, Turkey
[2] Department of Mechanical and Aerospace Engineering, Missouri University of Science and Technology, Rolla, Missouri, USA
[3] Mechanical Engineering Department, Turkish-German University, Istanbul, Turkey
[4] Intelligence System Center, Missouri University of Science and Technology, Rolla, Missouri, USA
[5] Mechanical Engineering Department, Sakarya University, Sakarya, Turkey

Abstract

Craniofacial bone defects (CFD) are among the most common bone defects, resulting from trauma, inflammatory diseases, infection, congenital deformities, and tumor resections. Bone tissue engineering scaffolds are an emerging solution to address the limited resources and technical challenges associated with the current standard of care for treating CFD, i.e., using autografts. In this study porous scaffolds are 3D printed using digital light processing (DLP) with slurries based on polylactic acid (PLA) resin incorporated with various ratios of hydroxyapatite (HA) and bioactive borate glass (BBG). The structure of 3D-printed scaffolds was characterized using X-ray diffraction (XRD), Fourier transmission infrared (FTIR) spectroscopy, and scanning electron microscopy. We investigated the effect of scaffold composition on the mechanical properties, shape fidelity, and degradation rate. Our results showed that addition of HA affects the viscosity of PLA more than BBG. The highest contact angle was found in PLA-HA10 scaffolds and the lowest in PLA-BBG20 as 81.4 ° and 69.7°, respectively. Findings from this research provide insight on the capability of DLP for fabrication of polymer-ceramic scaffolds for CFD treatment.

Keywords: Craniofacial bone, bone tissue engineering, digital light processing, polylactic acid, hydroxyapatite, bioactive glass.

1. Introduction

Craniofacial defects (CFDs) are among the most common bone defects caused by traumatic injuries, inflammatory and infectious diseases, congenital malformations, tumor resection, and bone resorption after tooth extraction or periodontal disease [1,2]. Each year approximately 200,000 CFDs occur in the United States, 6% of which require bone transplantation with an economic burden of ~$2 billion [3,4]. Cranioplasty is a neurosurgical procedure to reconstruct cranial defects. Reconstructive surgeons prefer to use autograft and allograft bones first in the reconstruction of critical cranial defects [5,6]. More than 2 million bone grafts take place each year around the world (500,000 in the U.S.), making bone the second most common transplant tissue after blood tissue [4,7,8]. However, their use faces major shortcomings, including limited source, morbidity, adverse immune response, graft rejection, transmission of diseases, and secondary trauma [9,10]. Biomaterial-based scaffolds are being developed as alternatives to autografts and allografts to address these challenges [10,11].

Scaffolds are expected to be biocompatible, bioactive, porous, and osteoconductive. They should also possess mechanical properties that mimic natural bone to promote optimal bone growth. The design and material selection for a scaffold are crucial determinants of its biomechanical and biological performance [12,13]. Polylactic acid (PLA), polymethyl methacrylate (PMMA), polyether ether ketone (PEEK), polyethylene, titanium and hydroxyapatite (HA) and calcium phosphate ceramics, collagen, gelatin, chitosan and alginate are most used synthetic biomaterials in bone tissue engineering (BTE) [14–18]. PLA is a biocompatible and biodegradable polymer that has been approved for specific medical applications by the U.S. Food and Drug Administration [19]. PLA can be used in temporary scaffold implants, drug delivery and various tissue engineering scaffolds due to biocompatible, biodegradable, nontoxicity and bioresorbable properties [20,21]. However, the lack of reactive side chain groups and the low hydrophilicity of PLA result in a low affinity for cells and low interaction between the scaffold and the surrounding tissue [22]. Osteoconductivity of PLA can be improved by adding bioceramics such as Hydroxyapatite (HA) and bioactive borate glass (BBG). HA is a highly effective bone repair material due to its close resemblance to natural bone's mineral component, promoting new bone growth through its osteoconductive properties. However, the low solubility of pure HA leads to slow degradation and resorption that can hinder new bone formation [23]. BBG, a bioactive material, has gained significant attention in bone tissue engineering because of its outstanding biodegradability and osteogenic properties [24]. Ions, especially silica, calcium and sodium, which positively influence bone regeneration and vascularization, are released when BBG is dissolved in biological fluids [23]. When BBG is submerged in tissue, it reacts with physiological fluids and forming a hydroxyapatite layer on the surface of scaffold, which leads to higher bone regeneration [24–26]. The three-dimensional (3D) pore architecture of scaffolds is another critical factor that influences their mechanical properties, cell infiltration, migration, adhesion, vascularization and nutrient diffusion during bone healing [27–29]. Scaffolds with a wide range of pore sizes from 10 to 2,250 μm have been successfully fabricated for bone tissue engineering (BTE) applications [30–32]. Previous studies have shown that micropores (100 to 300 μm) are optimal for osteoblast proliferation by providing more surface area for protein adhesion and cell attachment [27,33]. Macropores larger than 300 μm are essential for bone growth.

Recently additive manufacturing techniques have been used in fabrication of scaffolds [34], demonstrating their ability to fabricate FGM scaffolds with varying shapes and sizes [35,36] . Digital light processing (DLP) is an additive manufacturing technique that has the ability to fabricate complex geometry with high resolution (50 - 100 μm layer thickness) [37,38]. In this method a liquid photopolymer resin is solidified layer by layer with a digital light projector. DLP 3D printers can be used to fabricate porous scaffolds by mixing the photopolymer resin with ceramics and biopolymers. The ability to produce scaffolds with various pore structures and compositions makes DLP one of the most favored production methods in BTE. Zhang et al. have fabricated CaP scaffolds with well-controlled multi-level porous and nanoscale internal structures [39]. In another study, scaffold suspensions were prepared by mixing photocurable polymer with fluorcanasite glass ceramic particles at various loading levels [37]. Scaffolds with uniform pore (650 μm) microarchitecture and interconnected porosity were fabricated successfully. Pore size and pore distribution can be well controlled in the DLP Method.

Although ceramic enhanced polymer composites have been extensively investigated, there have been few studies on DLP-based 3D printing of biodegradable PLA, HA and BBG composites. This study presents the development of novel scaffolds with different material composition that have been specifically designed for the regeneration of cranial bone. Scaffolds with 650 μm pore size were fabricated with varying amounts of HA and BBG ceramics blended

with PLA resin. The microstructure, contact angle, mechanical strength, bioactivity and degradation rates were investigated.

2. Materials and Methods

2.1. Materials

Polylactic Acid (PLA) resin was purchased from Uniformation (Shenzhen, China) and Hydroxyapatite (HA) was purchased from Sigma Aldrich (Missouri, USA). Bioactive borate glass (BBG 1605, microspheres at particle size <20 μm) was supplied by ETS Wound Care (Missouri, USA). BBG is composed of 51.6 wt.% B_2O_3, 20 wt.% CaO, 6 wt.% Na_2 O, 5 wt.% MgO, 4 wt.% P_2O_5, 12 wt.% K_2O, 1 wt.% ZnO, and 0.4 wt.% CuO. Deionized water was used in biomaterial ink preparation and other experiments.

2.2. Fabrication of scaffolds

The slurries for fabricating scaffolds were prepared by adding different weight/volume percentages (wt./v%, g/ml) of HA and BBG powders to photo-curable PLA resin. The different formulations included: 10 wt./v% HA, 10 wt./v% HA + 10 wt./v% BBG and 20 wt./v% BBG. The mixtures were then homogenized using a magnetic stirrer.

The scaffolds were designed with SolidWorks software and the model files were converted to the .STL (Standard Triangulation Language) file. The porous samples have the dimensions of 8 x 8 x 8 mm^3 with a pore size of 650 μm.

Anycubic Photon 5M was used to fabricate the scaffolds. First, .STL files were imported into slicing software to generate G-code defining the scaffold printing pattern. Then, the prepared slurries were poured into the resin tank to print the scaffolds. The printing parameters set in our study were: layer thickness = 50 μm, exposure time = 2.7 s and off time 3s. Following the printing, the scaffolds were cleaned with isopropyl alcohol and subjected to airflow through their pores to remove uncured slurry. The samples were then placed under UV light to improve the overall strength and quality of scaffold.

2.3. Characterization

The slurry's rheological behavior was assessed using Kinexus Ultra+ (Malvern Panalytical Ltd., Malvern, U.K.), a rotational rheometer. Viscosity and shear rate curves were obtained for comparison and analysis of the rheological properties of the scaffold slurries. All measurements were carried out at room temperature (24 °C), with the shear rate ramped up from 0 s^{-1} to 100 s^{-1}. Helios Hydra DualBeam, a scanning electron microscope, was used to characterize the scaffold's morphology and surface microstructure. Samples were mounted in a holder with double insulated tape and coated with gold before SEM analysis. X-ray diffraction (XRD) was measured with Rigaku Smartlab at a scanning rate of 10°/min and 2θ values from 20° to 60° to analyze the phase composition of the scaffold. Fourier transform infrared spectroscopy was performed by using a Nicolet iS50 spectrophotometer in the mid-IR range (4000 – 400 cm^{-1}) to examine the chemical bonds between PLA, HA and BBG.

The water contact angles of the scaffolds were measured by applying 5 μL water droplets to the scaffold surfaces and imaging the droplets after 5 seconds. Three replicates per sample variation were run for each composition.

The compressive strengths of scaffolds (dimensions: 8×8×8 mm^3) were measured using an MTS universal testing machine with the loading speed of 1 mm/min. Five samples were tested for each scaffold. The average and standard deviation of the five samples were calculated from the measured data.

Apatite formation on a scaffold in simulated body fluid (SBF) is useful for predicting the material's *in vivo* bone bioactivity. The bioactivity of scaffold was evaluated by immersing the scaffold samples in SBF for 4 weeks. Afterwards, the samples were dried at room temperature and kept in a closed container before characterization.

3. Results and discussion

3.1. Rheological evaluation of slurry

The SEM micrograph of HA and BBG powders and the viscosity-shear rate graph for four different compositions of slurry are shown in Figure 1. BBG powder has D50 around 14.27 μm and shows unimodal particle size distribution with a low range change of particle size. HA has a larger particle size range and a bimodal size distribution with D50 around 9.99 μm.

The rheological behavior of the scaffold slurry is a critical factor influencing the printability of slurry in the DLP method. The slurry should be able to move and spread out easily in the print vat. High viscosity can make it difficult for the slurry to flow back into the print tank and can cause particles in the slurry to deposit onto the previous layer, after the print head has passed, leading to printing inaccuracy [38,40]. Adding ceramic fillers into a photosensitive resin typically causes a significant increase in the viscosity of the resulting slurry [41,42]. This increase can be attributed to a number of factors, including increased internal friction between the particles, impeded resin flow due to particle packing, potential trapping of the resin within the filler network, and different particle sizes incorporated into resin [38]. In this study we incorporated the HA and BBG into the PLA-based resin. The viscosity-shear rate graph for different compositions of slurry was assessed for different compositions of slurry by rheological measurements. The PLA resin without any additives had the lowest viscosity, while the PLA-HA10 slurry had the highest viscosity. The addition of HA powder greatly increased the viscosity of the slurry and made it a shear-thinning fluid. However, BBG powder does not change the rheological behavior of the resin significantly. It was also observed that the addition of BBG to the PLA-HA10 slurry had a viscosity reduction effect. The high solubility of BBG, powder size and chemical reactions between composition ingredients can lead to the reduction of viscosity [43]. The viscosity of slurry affects the pore size, pore shape and shape fidelity of the fabricated scaffolds.

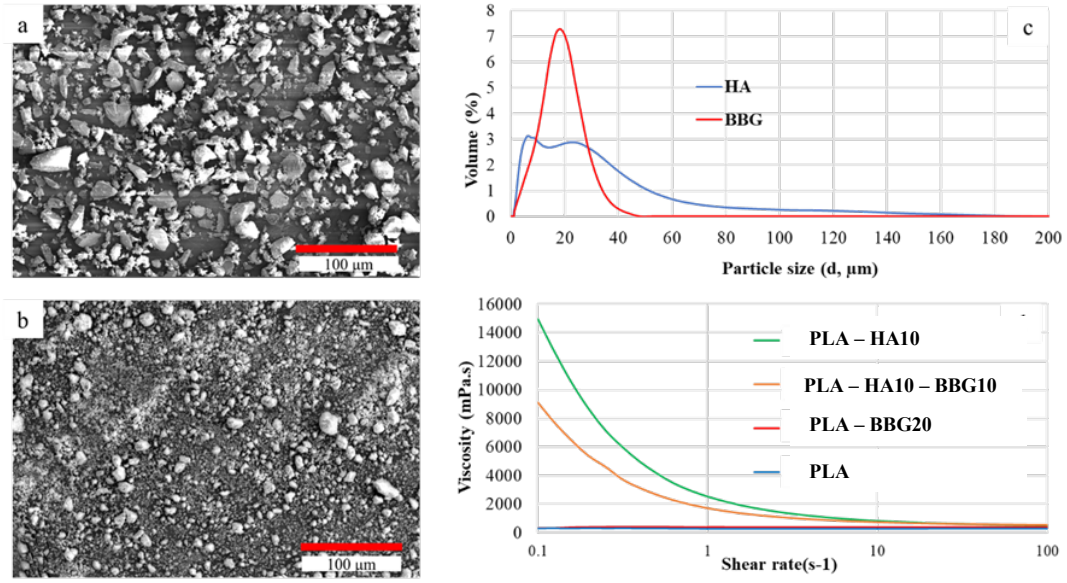

Figure 1. SEM micrograph of (a) HA and (b) BBG, (c) particle size distribution of HA and BBG, and (d) viscosity vs. shear rate of PLA, PLA-10HA, PLA-10HA-10BBG and PLA-20BBG slurries.

3.2. Scaffold microstructure

The shapes of the cranial bone defects can be very different, depending on the cause, the size and the location. A customizable, high-precision bone graft substitute is necessary to ensure the integrity of the bone defect repair and preservation of the original contour shape [44]. Figure 2 presents the optical micrographs and SEM images of scaffold surfaces for various scaffolds fabricated using a DLP 3D printer with different material compositions including PLA, PLA-HA10, PLA-HA10-BBG10, and PLA-BBG20. The average pore size, pore area, pore perimeter, and shape fidelity of the fabricated scaffolds are shown in Table 1. The pore size of scaffold printed with pure PLA is larger than the designed size and the other scaffolds. The mean pore size of PLA scaffold was 666.7 ± 12.5 µm. Note that curing causes a resin material to shrink by narrowing the molecular gaps, consequently enlarging the pores by incorporating this space into the material volume [45,46]. The pore size of scaffold fabricated with the PLA-HA10 blend was 571.3 ± 26.5 µm, which is smaller than the designed size. PLA-HA10 composites have smaller pore sizes due to the rheological behavior of PLA. The decrease in the precision of the scaffold is caused by the lower viscosity and light reflection of HA particles in the PLA/HA resin [47]. The high viscosity of PLA-HA10 blend reduces the ability of the slurry to spread in the resin tank and reduces the ability of the uncured slurry to flow through the pores and cause HA powder to deposit on the printed layers [48]. The pore size of the PLA-HA10-BBG10 scaffolds increased from that of PLA-HA10 to 612 ± 24.7 µm. This is because incorporating BBG powder into the PLA-HA10 slurry resulted in reduced viscosity and improved flow. The pore sizes of the PLA -HA10-BBG10 and PLA-BBG20 scaffolds are close to each other, with the lower viscosity of PLA-BBG20 resulting in a lightly larger pore size of 622 ± 25.1 µm.

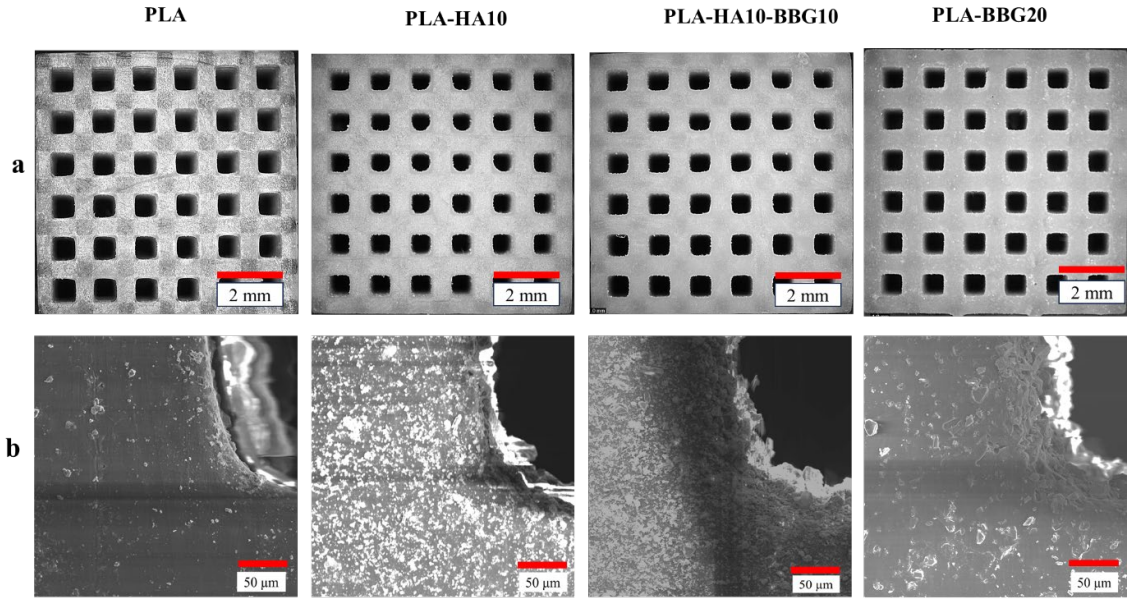

Figure 2. Microstructure of the scaffolds PLA, PLA-10HA, PLA-10HA-10BBG and PLA-20BBG **a)** Optical micrographs **b)** SEM images of scaffold surfaces.

Table 1. The average pore size of scaffolds.

	Pore size (µm)	
	Mean	**SD**
PLA	666.7	12.5
PLA-HA10	571.3	26.5
PLA-HA10-BBG10	612.9	24.7
PLA-BBG20	622.6	25.1

The details of microstructure and surface of the scaffolds were measured using scanning electron microscopy (SEM), which allows visualizing the distribution and precipitation of the HA particles during the DLP printing process. It appears that the PLA-HA10 scaffold has higher surface roughness than the other scaffolds. The XRD patterns of the scaffolds fabricated with the four different material compositions are shown in Figure 3. Neither PLA nor PLA-BBG20 show any characteristic peaks in the XRD pattern, suggesting that both materials have an amorphous structure. X-ray diffraction (XRD) analysis showed peaks at 2θ values of 25.9°, 31.9° and 33.0°, corresponding to the standard patterns for the crystalline hydroxyapatite (HA) phase. XRD analysis of the PLA-HA10 and PLA-HA10-BBG10 scaffolds revealed peaks consistent with the reference pattern for pure hydroxyapatite in the standard phase (JCPDS # 09-0432). Figure 4 shows the FTIR spectra of the PLA, PLA-HA10, PLA-HA10-BBG10 and PLA-BBG20 scaffolds. The characteristic C–O–C, C-H, C=O and O-H peaks of the PLA can be seen at around 1192, 1406, 1719, 2928 and 3350 cm^{-1} [49]. The FTIR spectra show

characteristic peaks at 567 cm-¹ and 809 cm-¹, which correspond to the fundamental bending and stretching vibrations of the PO_4^{3-} groups in HA, respectively [50].

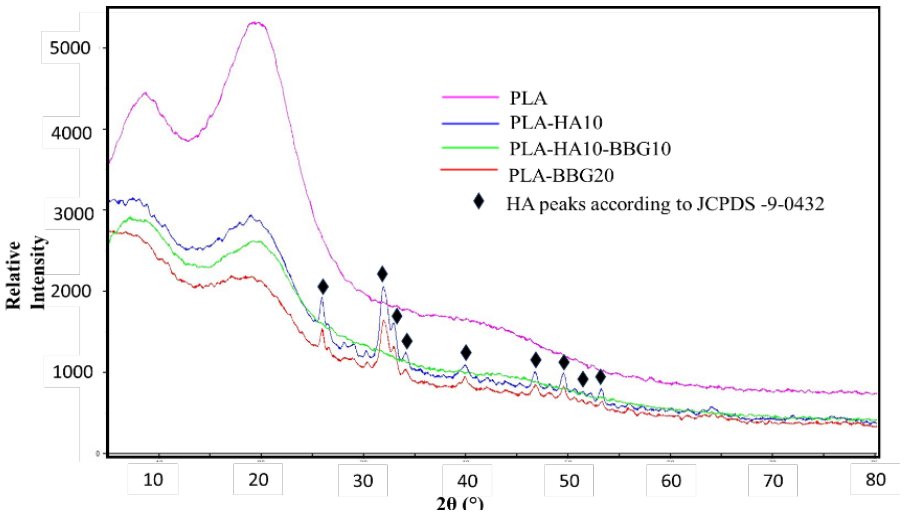

Figure 3. X-Ray Diffraction (XRD) pattern of pure PLA, PLA-HA10, PLA-HA10-BBG10 and PLA-BBG20 scaffolds.

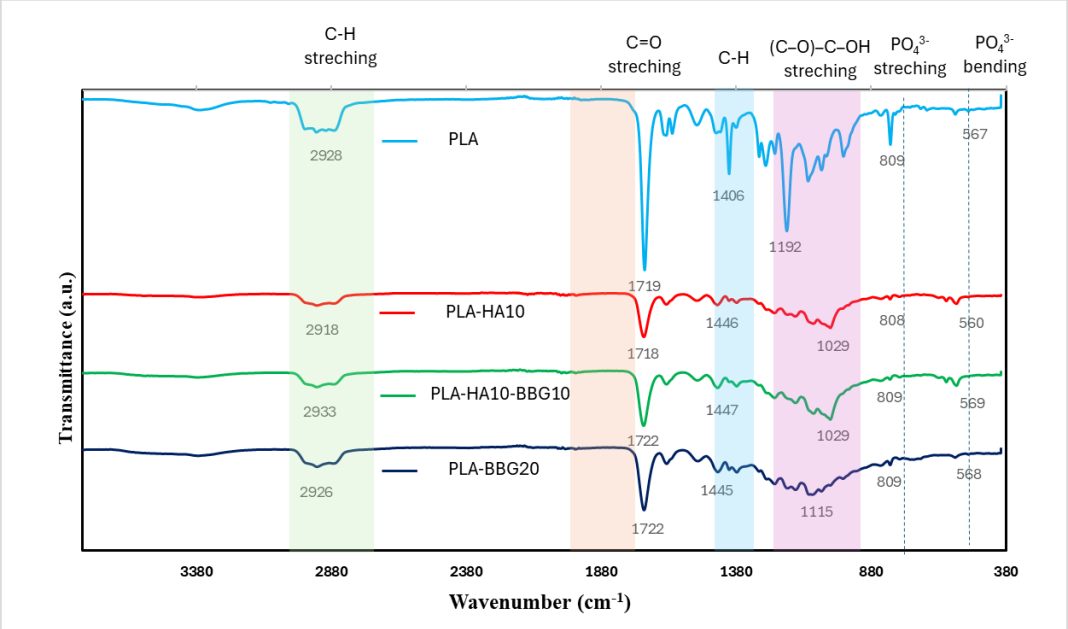

Figure 4. FTIR spectra of PLA, PLA-HA10, PLA-HA10-BBG10, and PLA-BBG20 scaffolds.

3.3. Compressive strength

The scaffolds should be strong enough to integrate seamlessly with the surrounding bone and to maintain the structural integrity necessary for successful bone repair. The compressive strength of the non-porous blocks for different material compositions and the porous scaffolds made of PLA-HA10 are shown in Figure 5. The addition of HA and BBG ceramics increases the compressive strength of the composite scaffolds. The compressive strength of PLA-HA10 scaffold, measured 64.4 MPa, is higher than the compressive strengths of PLA-HA10-BBG10

and PLA-BBG20 scaffolds. The addition of BBG to the PLA-HA10 composite decreases the strength of the scaffolds. The compressive strength of the porous scaffolds (10.4 MPa - 12.04 MPa) is within the range of cancellous bone (0.1 MPa - 16 MPa) [51]. This suggests that these scaffolds can be suitable for use in applications in which they are required to withstand compressive loads similar to those of cancellous bone.

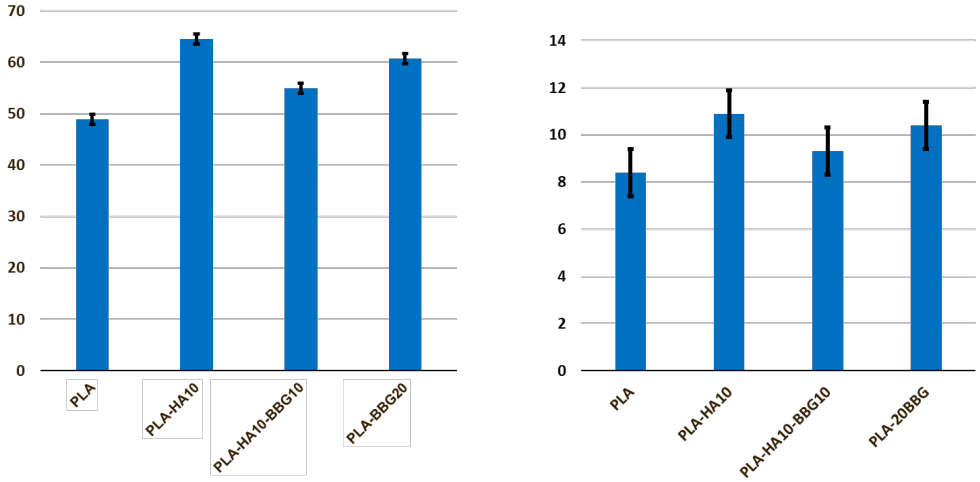

Figure 5. Compressive strength of scaffolds: a) non-porous blocks fabricated with different material compositions, b) porous scaffolds fabricated with different material compositions. The unit of compressive strength is MPa.

3.4. Contact angle

The hydrophilic surface properties of the scaffolds affect the cell adhesion of the scaffolds [24]. PLA has low hydrophilicity, resulting in poor wettability, which implies lack of cell attachment and interaction between the scaffold and surrounding tissues [52]. Figure 6 shows the images and data statistics of water contact angle measurement for PLA, PLA-HA10, PLA-HA10-BBG10, and PLA-BBG20 scaffolds. The contact angle of the scaffolds increases with the addition of HA and decreases with the addition of BBG. The lowest contact angle is 69.7° for PLA-BBG20 scaffold.

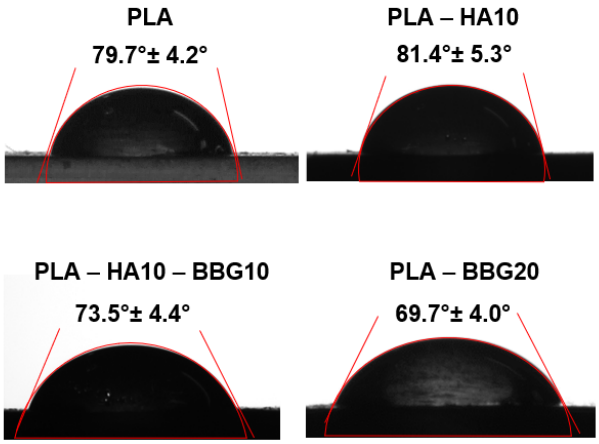

Figure 6. Images and statistics of water contact angle measurement for PLA PLA-HA10, PLA-HA10-BBG10, and PLA-BBG20 scaffolds.

3.5. Bioactivity of scaffold upon soaking in SBF

The SEM micrographs and EDS results of the scaffolds immersed in SBF for 4 weeks are shown in Figure 7. The mineralized apatite growth and salt can be seen on the surface of the scaffolds, which can be confirmed by EDS analysis. Energy-dispersion X-ray spectroscopy (EDS) analysis revealed the presence of calcium (Ca) and phosphorus (P) on the surfaces of PLA-HA10 and PLA-BBG20 scaffolds. In contrast, the PLA scaffold showed minimal calcium and phosphorus, suggesting poor HA formation on its surface. In the same line with other research work, PLA has a poor bioactivity due to its hydrophobic nature [13,53] . The formation of HA is dependent on several factors, including the pH of the medium, the adsorption and release of ions at the interface, surface roughness, and the wettability [54–56].

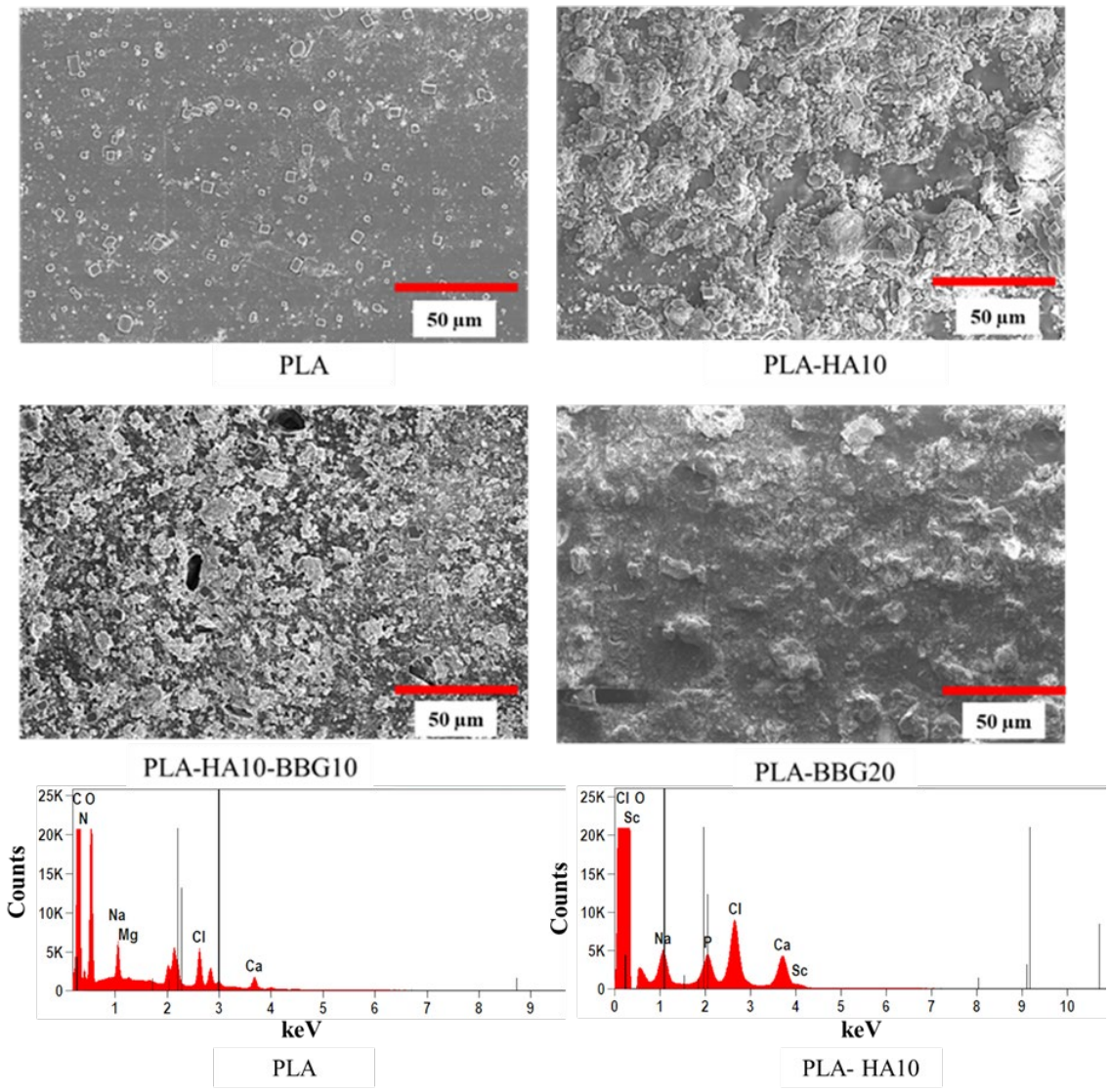

Figure 7. SEM micrograph of scaffolds (PLA, PLA-HA10, PLA-HA10-BBG10 and PLA-BBG20) and EDS analysis of PLA and PLA-HA10 scaffolds.

4. Conclusion

3D printing by Digital Light Processing (DLP) is ideal for fabrication of scaffolds with intricate structures due to its high resolution and precision fabrication capabilities. The physical and biological properties of scaffolds can be improved by incorporation other biomaterials. In this study, PLA resin was blended with different ratios of HA and BBG ceramics to fabricate porous scaffolds with DLP for the regeneration of cranial bone. The rheological properties of the slurry affect the printability of the slurry. Incorporating HA significantly affected the rheological properties of the PLA resin, resulting in reduced printability, while incorporating BBG changes the viscosity of the PLA resin slightly. It can be seen that PLA-HA10 scaffold has the smallest pore size and PLA scaffold has largest pore size. PLA-BBG20 has the lowest contact angle, with a value of 69.7°, among the various material compositions used in the study. A lower contact angle may increase cell adhesion and proliferation. This is beneficial for new bone formation. Apatite formation is another important factor in bone repair. The apatite formation on scaffolds fabricated with HA and BBG ceramics was better compared with pure PLA. Although pure PLA has higher printability, the surface properties and bioactivity of PLA scaffold is lower compared to the other scaffolds. The weak features of PLA for bone regeneration have been improved with the use of HA and BBG.

References

[1] J. Li, C. Gsaxner, A. Pepe, A. Morais, V. Alves, G. von Campe, J. Wallner, J. Egger, Synthetic skull bone defects for automatic patient-specific craniofacial implant design, Sci. Data 8 (2021) 1–8. https://doi.org/10.1038/s41597-021-00806-0.

[2] G. Lu, Y. Xu, Q. Liu, M. Chen, H. Sun, P. Wang, X. Li, Y. Wang, X. Li, X. Hui, E. Luo, J. Liu, Q. Jiang, J. Liang, Y. Fan, Y. Sun, X. Zhang, An instantly fixable and self-adaptive scaffold for skull regeneration by autologous stem cell recruitment and angiogenesis, Nat. Commun. 13 (2022) 1–20. https://doi.org/10.1038/s41467-022-30243-5.

[3] B. Gaihre, S. Uswatta, A. Jayasuriya, Reconstruction of Craniomaxillofacial Bone Defects Using Tissue-Engineering Strategies with Injectable and Non-Injectable Scaffolds, J. Funct. Biomater. 8 (2017) 49. https://doi.org/10.3390/jfb8040049.

[4] R. Zhao, R. Yang, P.R. Cooper, Z. Khurshid, A. Shavandi, J. Ratnayake, Bone grafts and substitutes in dentistry: A review of current trends and developments, Molecules 26 (2021) 1–27. https://doi.org/10.3390/molecules26103007.

[5] O. Kordi, A.H. Behravesh, S. Hasannia, S.K. Hedayati, M. Pourghaumi, M. Mazdi, I. Ghaderi, G. Rizvi, Additive manufacture of PLLA scaffolds reinforced with graphene oxide nano-particles via digital light processing (DLP), J. Biomater. Appl. 38 (2023) 484–499. https://doi.org/10.1177/08853282231202734.

[6] B. Xu, P. Zheng, F. Gao, W. Wang, H. Zhang, X. Zhang, X. Feng, W. Liu, A Mineralized High Strength and Tough Hydrogel for Skull Bone Regeneration, Adv. Funct. Mater. 27 (2017). https://doi.org/10.1002/adfm.201604327.

[7] C.E. Gillman, A.C. Jayasuriya, FDA-approved bone grafts and bone graft substitute devices in bone regeneration, Mater. Sci. Eng. C 130 (2021) 112466. https://doi.org/10.1016/j.msec.2021.112466.

[8] J.T.B. Ratnayake, M. Mucalo, G.J. Dias, Substituted hydroxyapatites for bone regeneration: A review of current trends, J. Biomed. Mater. Res. - Part B Appl. Biomater. 105 (2017) 1285–1299. https://doi.org/10.1002/jbm.b.33651.

[9] M. Altunbek, S.F. Afghah, A. Fallah, A.A. Acar, B. Koc, Design and 3D Printing of Personalized Hybrid and Gradient Structures for Critical Size Bone Defects, ACS Appl. Bio Mater. (2023). https://doi.org/10.1021/acsabm.3c00107.

[10] T. Distler, N. Fournier, A. Grünewald, C. Polley, H. Seitz, R. Detsch, A.R. Boccaccini, Polymer-Bioactive Glass Composite Filaments for 3D Scaffold Manufacturing by Fused Deposition Modeling: Fabrication and Characterization, Front. Bioeng. Biotechnol. 8 (2020) 1–17. https://doi.org/10.3389/fbioe.2020.00552.

[11] M.R. Senra, M. de F. Vieira Marques, Synthetic polymeric materials for bone replacement, J. Compos. Sci. 4 (2020). https://doi.org/10.3390/jcs4040191.

[12] Y. Bai, Z. Wang, X. He, Y. Zhu, X. Xu, H. Yang, G. Mei, S. Chen, B. Ma, R. Zhu, Application of Bioactive Materials for Osteogenic Function in Bone Tissue Engineering, Small Methods 2301283 (2024) 1–27. https://doi.org/10.1002/smtd.202301283.

[13] L.R. Jaidev, K. Chatterjee, Surface functionalization of 3D printed polymer scaffolds to augment stem cell response, Mater. Des. 161 (2019) 44–54. https://doi.org/10.1016/j.matdes.2018.11.018.

[14] J.H. Ahn, J. Kim, G. Han, D.E. Kim, K.H. Cheon, H. Lee, H.E. Kim, Y.J. Kim, T.S. Jang, H. Do Jung, 3D-printed biodegradable composite scaffolds with significantly enhanced mechanical properties via the combination of binder jetting and capillary rise infiltration process, Addit. Manuf. 41 (2021) 101988. https://doi.org/10.1016/j.addma.2021.101988.

[15] H. Kim, G.H. Yang, C.H. Choi, Y.S. Cho, G.H. Kim, Gelatin/PVA scaffolds fabricated using a 3D-printing process employed with a low-temperature plate for hard tissue regeneration: Fabrication and characterizations, Int. J. Biol. Macromol. 120 (2018) 119–127. https://doi.org/10.1016/j.ijbiomac.2018.07.159.

[16] O. Omar, T. Engstrand, L.K.B. Linder, J. Åberg, F.A. Shah, A. Palmquist, U. Birgersson, I. Elgali, M. Pujari-Palmer, H. Engqvist, P. Thomsen, In situ bone regeneration of large cranial defects using synthetic ceramic implants with a tailored composition and design, Proc. Natl. Acad. Sci. U. S. A. 117 (2020) 26660–26671. https://doi.org/10.1073/pnas.2007635117.

[17] K. Aoki, H. Ideta, Y. Komatsu, A. Tanaka, M. Kito, M. Okamoto, J. Takahashi, S. Suzuki, N. Saito, Bone-Regeneration Therapy Using Biodegradable Scaffolds : Calcium Phosphate Bioceramics and Biodegradable Polymers, Bioeng. 2024, (2024).

[18] B. Nim, S.S. Rahayu, K. Thananukul, C. Eang, M. Opaprakasit, A. Petchsuk, C. Kaewsaneha, D. Polpanich, P. Opaprakasit, Sizing down and functionalizing polylactide (PLA) resin for synthesis of PLA - based polyurethanes for use in biomedical applications, Sci. Rep. (2023) 1–20. https://doi.org/10.1038/s41598-023-29496-x.

[19] R. Agarwal, J. Singh, V. Gupta, Predicting the compressive strength of additively manufactured PLA-based orthopedic bone screws: A machine learning framework, Polym. Compos. 43 (2022) 5663–5674. https://doi.org/10.1002/pc.26881.

[20] W. Xu, A. Pranovich, P. Uppstu, X. Wang, D. Kronlund, J. Hemming, H. Öblom, N.

Moritz, M. Preis, N. Sandler, S. Willför, C. Xu, Novel biorenewable composite of wood polysaccharide and polylactic acid for three dimensional printing, Carbohydr. Polym. 187 (2018) 51–58. https://doi.org/10.1016/j.carbpol.2018.01.069.

[21] F. Alam, V.R. Shukla, K.M. Varadarajan, S. Kumar, Microarchitected 3D printed polylactic acid (PLA) nanocomposite scaffolds for biomedical applications, J. Mech. Behav. Biomed. Mater. 103 (2020) 103576. https://doi.org/10.1016/j.jmbbm.2019.103576.

[22] V.V. Nayak, V. Sanjairaj, R.K. Behera, J.E. Smay, N. Gupta, P.G. Coelho, L. Witek, Direct inkjet writing of polylactic acid/β-tricalcium phosphate composites for bone tissue regeneration: A proof-of-concept study, J. Biomed. Mater. Res. Part B Appl. Biomater. 112 (2024). https://doi.org/10.1002/jbm.b.35402.

[23] A.K. Rajendran, M.S.J. Anthraper, N.S. Hwang, J. Rangasamy, Osteogenesis and angiogenesis promoting bioactive ceramics, Mater. Sci. Eng. R Reports 159 (2024). https://doi.org/10.1016/j.mser.2024.100801.

[24] J. Han, J. Wu, X. Xiang, L. Xie, R. Chen, L. Li, K. Ma, Q. Sun, R. Yang, T. Huang, L. Tong, L. Zhu, H. Wang, C. Wen, Y. Zhao, J. Wang, Biodegradable BBG/PCL composite scaffolds fabricated by selective laser sintering for directed regeneration of critical-sized bone defects, Mater. Des. 225 (2023) 111543. https://doi.org/10.1016/j.matdes.2022.111543.

[25] S. Mistry, D. Kundu, S. Datta, D. Basu, Comparison of bioactive glass coated and hydroxyapatite coated titanium dental implants in the human jaw bone, Aust. Dent. J. 56 (2011) 68–75. https://doi.org/10.1111/j.1834-7819.2010.01305.x.

[26] A.A. Aslam, J. Akram, R.A. Mehmood, A. Mubarak, A. Khatoon, U. Akbar, S.A. Ahmad, M. Atif, Boron-based bioactive glasses: Properties, processing, characterization and applications, Ceram. Int. 49 (2023) 19595–19605. https://doi.org/10.1016/j.ceramint.2023.03.164.

[27] N. Abbasi, S. Hamlet, R.M. Love, N. Nguyen, Porous scaffolds for bone regeneration, J. Sci. Adv. Mater. Devices 5 (2020) 1–9. https://doi.org/10.1016/j.jsamd.2020.01.007.

[28] C.M. Murphy, Understanding the effect of mean pore size on cell activity in collagen-glycosaminoglycan scaffolds, (2010) 377–381. https://doi.org/10.4161/cam.4.3.11747.

[29] J.M. Sobral, S.G. Caridade, R.A. Sousa, J.F. Mano, R.L. Reis, Three-dimensional plotted scaffolds with controlled pore size gradients : Effect of scaffold geometry on mechanical performance and cell seeding efficiency, Acta Biomater. 7 (2011) 1009–1018. https://doi.org/10.1016/j.actbio.2010.11.003.

[30] T. Ghahri, Z. Salehi, S. Aghajanpour, M.B. Eslaminejad, N. Kalantari, M. Akrami, R. Dinarvand, H.L. Jang, M. Esfandyari-Manesh, Development of osteon-like scaffold-cell construct by quadruple coaxial extrusion-based 3D bioprinting of nanocomposite hydrogel, Biomater. Adv. 145 (2023) 213254. https://doi.org/10.1016/j.bioadv.2022.213254.

[31] C. Paredes, F.J. Martínez-Vázquez, A. Pajares, P. Miranda, Co-continuous calcium phosphate/polycaprolactone composite bone scaffolds fabricated by digital light processing and polymer melt suction, Ceram. Int. 47 (2021) 17726–17735. https://doi.org/10.1016/j.ceramint.2021.03.093.

[32] S.M.M. Roosa, J.M. Kemppainen, E.N. Moffitt, P.H. Krebsbach, S.J. Hollister, The pore size of polycaprolactone scaffolds has limited influence on bone regeneration in an in vivo model, (2009). https://doi.org/10.1002/jbm.a.32381.

[33] T.C. Lim, K.S. Chian, K.F. Leong, Cryogenic prototyping of chitosan scaffolds with controlled micro and macro architecture and their effect on in vivo neo-vascularization and cellular infiltration, J. Biomed. Mater. Res. - Part A 94 (2010) 1303–1311. https://doi.org/10.1002/jbm.a.32747.

[34] K.S. Prakash, T. Nancharaih, V.V.S. Rao, Additive Manufacturing Techniques in Manufacturing -An Overview, Mater. Today Proc. 5 (2018) 3873–3882. https://doi.org/10.1016/j.matpr.2017.11.642.

[35] H. Shi, P. Zhou, J. Li, C. Liu, L. Wang, Functional Gradient Metallic Biomaterials: Techniques, Current Scenery, and Future Prospects in the Biomedical Field, Front. Bioeng. Biotechnol. 8 (2021). https://doi.org/10.3389/fbioe.2020.616845.

[36] I.M. El-Galy, B.I. Saleh, M.H. Ahmed, Functionally graded materials classifications and development trends from industrial point of view, SN Appl. Sci. 1 (2019) 1378. https://doi.org/10.1007/s42452-019-1413-4.

[37] A. Vyas, S. Bandhu Ghosh, S. Bandyopadhyay-Ghosh, A.K. Agrawal, D. Khare, A.K. Dubey, Digital light processing mediated 3D printing of biocomposite bone scaffolds: Physico-chemical interactions and in-vitro biocompatibility, Polym. Compos. 43 (2022) 3175–3188. https://doi.org/10.1002/pc.26609.

[38] Y. Wang, S. Chen, H. Liang, Y. Liu, J. Bai, M. Wang, Digital light processing (DLP) of nano biphasic calcium phosphate bioceramic for making bone tissue engineering scaffolds, Ceram. Int. 48 (2022) 27681–27692. https://doi.org/10.1016/j.ceramint.2022.06.067.

[39] B. Feng, M. Zhang, C. Qin, D. Zhai, Y. Wang, Y. Zhou, J. Chang, Y. Zhu, C. Wu, 3D printing of conch-like scaffolds for guiding cell migration and directional bone growth, Bioact. Mater. 22 (2023) 127–140. https://doi.org/10.1016/j.bioactmat.2022.09.014.

[40] Z. Liu, H. Liang, T. Shi, D. Xie, R. Chen, X. Han, L. Shen, C. Wang, Z. Tian, Additive manufacturing of hydroxyapatite bone scaffolds via digital light processing and in vitro compatibility, Ceram. Int. 45 (2019) 11079–11086. https://doi.org/10.1016/j.ceramint.2019.02.195.

[41] D. Komissarenko, S. Roland, B.S.M. Seeber, T. Graule, DLP 3D printing of high strength semi-translucent zirconia ceramics with relatively low-loaded UV-curable formulations, Ceram. Int. 49 (2023) 21008–21016. https://doi.org/10.1016/j.ceramint.2023.03.236.

[42] S. Mamatha, P. Biswas, R. Johnson, Digital light processing of ceramics : an overview on process , materials and challenges, Prog. Addit. Manuf. 8 (2023) 1083–1102. https://doi.org/10.1007/s40964-022-00379-3.

[43] F. Fayyazbakhsh, M. H. Tusar, Y.-W. Huang, M. C. Leu, Effect of bioactive borate glass on printability and physical properties of hydrogels, Mater. Sci. Addit. Manuf. 3 (2024) 2845. https://doi.org/10.36922/msam.2845.

[44] J. Zhang, D. Huang, S. Liu, X. Dong, Y. Li, H. Zhang, Z. Yang, Q. Su, W. Huang, W. Zheng, W. Zhou, Zirconia toughened hydroxyapatite biocomposite formed by a DLP 3D

printing process for potential bone tissue engineering, Mater. Sci. Eng. C 105 (2019) 110054. https://doi.org/10.1016/j.msec.2019.110054.

[45] Q. Zhang, S. Weng, C.M. Hamel, S.M. Montgomery, Design for the reduction of volume shrinkage-induced distortion in digital light processing 3D printing, Extrem. Mech. Lett. 48 (2021) 101403. https://doi.org/10.1016/j.eml.2021.101403.

[46] Y. Jian, Y. He, T. Jiang, C. Li, W. Yang, J. Nie, Polymerization Shrinkage of (Meth) acrylate Determined by Reflective Laser Beam Scanning, J. Polym. Sci. PART B Polym. Phys. (2012) 923–928. https://doi.org/10.1002/polb.23086.

[47] D. Aki, S. Ulag, S. Unal, M. Sengor, N. Ekren, C. Lin, Y. Hakan, C. Bulent, D.M. Kalaskar, O. Gunduz, 3D printing of PVA / hexagonal boron nitride / bacterial cellulose composite scaffolds for bone tissue engineering, Mater. Des. 196 (2020) 109094. https://doi.org/10.1016/j.matdes.2020.109094.

[48] Y. Zeng, Y. Yan, H. Yan, C. Liu, P. Li, P. Dong, Y. Zhao, J. Chen, 3D printing of hydroxyapatite scaffolds with good mechanical and biocompatible properties by digital light processing, J. Mater. Sci. 53 (2018) 6291–6301. https://doi.org/10.1007/s10853-18-1992-2.

[49] J.P. Mofokeng, A.S. Luyt, T. Tábi, J. Kovács, Comparison of injection moulded, natural fibre-reinforced composites with PP and PLA as matrices, J. Thermoplast. Compos. Mater. 25 (2012) 927–948. https://doi.org/10.1177/0892705711423291.

[50] K.A.S. K. Alam, M. A. Gafur, Md. Hasan Mahmud, Chemical Characteristics of Hydroxyapatite from Oyster Shell by Thermo-Chemical Process, Int. J. Innov. Res. Sci. Eng. Technol. 04 (2015) 5039–5047. https://doi.org/10.15680/IJIRSET.2015.0407002.

[51] L.C. Gerhardt, A.R. Boccaccini, Bioactive glass and glass-ceramic scaffolds for bone tissue engineering, Materials (Basel). 3 (2010) 3867–3910. https://doi.org/10.3390/ma3073867.

[52] R. Donate, M. Monzón, M.E. Alemán-Domínguez, Additive manufacturing of PLA-based scaffolds intended for bone regeneration and strategies to improve their biological properties, E-Polymers 20 (2020) 571–599. https://doi.org/10.1515/epoly-2020-0046.

[53] P. Habibovic, In vitro and in vivo bioactivity assessment of a polylactic acid/hydroxyapatite composite for bone regeneration, Biomatter 4 (2014) e27664. https://doi.org/10.4161/biom.27664.

[54] H. Samadian, S. Farzamfar, A. Vaez, A. Ehterami, A. Bit, M. Alam, A. Goodarzi, G. Darya, M. Salehi, A tailored polylactic acid/polycaprolactone biodegradable and bioactive 3D porous scaffold containing gelatin nanofibers and Taurine for bone regeneration, Sci. Rep. 10 (2020) 1–12. https://doi.org/10.1038/s41598-020-70155-2.

[55] M. Mu, S. Liu, W. DeFlorio, L. Hao, X. Wang, K.S. Salazar, M. Taylor, A. Castillo, L. Cisneros-Zevallos, J.K. Oh, Y. Min, M. Akbulut, Influence of Surface Roughness, Nanostructure, and Wetting on Bacterial Adhesion, Langmuir 39 (2023) 5426–5439. https://doi.org/10.1021/acs.langmuir.3c00091.

[56] F. Fayyazbakhsh, M. Solati-Hashjin, A. Keshtkar, M.A. Shokrgozar, M.M. Dehghan, B. Larijani, Release behavior and signaling effect of vitamin D3 in layered double hydroxides-hydroxyapatite/gelatin bone tissue engineering scaffold: An in vitro evaluation, Colloids Surfaces B Biointerfaces 158 (2017) 697–708.

https://doi.org/10.1016/j.colsurfb.2017.07.004.

Acknowledgement

This work was supported by TÜBİTAK Directorate of Science Fellowships and Grant 2214 Programmes (BİDEB)